Theoretical calculation of pseudorotation rates applicable to the C_{60}^- ion

Ian D. Hands, Janette L. Dunn,* and Colin A. Bates
School of Physics and Astronomy, University of Nottingham, Nottingham, NG7 2RD, United Kingdom
(Received 2 February 2006; revised manuscript received 5 April 2006; published 22 June 2006)

The dynamical nature of the Jahn-Teller effect in the $T \otimes h$ Jahn-Teller system is explored theoretically using the time-evolution operator to obtain analytical expressions for the rate of pseudorotation between equivalent potential wells in the adiabatic potential energy surface as a function of the vibronic coupling parameters. We outline experiments that should be capable of measuring the pseudorotation rate in the C_{60}^- ion, and other systems derived from C_{60}. The theory presented here could then be combined with such data to probe the nature of the vibronic coupling in these fullerene systems.

DOI: 10.1103/PhysRevB.73.235425 PACS number(s): 61.48.+c, 31.30.Gs, 82.53.Uv

I. INTRODUCTION

The fullerene C_{60} and its ions, such as found in the fullerides, have been the subject of intense research for some years. In particular, materials containing fullerene ions have been found to show a range of interesting electrical, magnetic, and superconducting properties,[1–3] as well as exhibiting various structural and orientational phase transitions.[3–5] The mechanisms behind the various phenomena are not all completely understood. However, it seems highly likely that the intramolecular Jahn-Teller (JT) effect plays an important part in some of the processes, such as superconductivity in the A_3C_{60} fullerides.[3,6,7] Thus there is a clear need to investigate the nature and magnitude of the JT effect in all of the C_{60} ions. In this paper, we will consider JT effects applicable to C_{60}^- anions. These are amongst the simplest JT systems found in icosahedral symmetry (in that the electronic basis has the lowest dimension). Theoretical methods developed for this system can form a basis for further work on JT effects in more highly charged fullerene anions and cations.

Vibronic coupling distorts the C_{60}^- ion so that at any given instant it is in a configuration of reduced symmetry. This is known as a static JT effect. If only linear vibronic coupling is included, there is a continuous surface of equivalent minimum-energy points on the lowest adiabatic potential energy surface (APES).[8–10] The system will rotate between all of the equivalent minimum-energy points, resulting in a dynamic JT effect. This rotation of a distortion is usually referred to as a pseudorotation to distinguish it from real rotations of the fullerene ion. As all minimum points are sampled equally, this pseudorotation will produce a system whose symmetry is, on average, icosahedral. It is likely that in any real system (including the C_{60}^- ion), quadratic JT couplings[11,12] or other factors such as anharmonicity[13–15] or a pseudo-JT effect[16,17] will be present. In these cases, the minimum-energy points will form a set of several isoenergetic wells on the APES.[8,9,18] If the barriers between the wells are large in all directions in coordinate space, the system will tunnel between the wells. If they are small in some directions, the system will undergo hindered rotations in these directions. In both cases, the system will again exhibit the full icosahedral symmetry of the original C_{60}^- ion on average. As tunneling, hindered rotations and "pure" pseudorotations can be viewed as different limits of each other, all three situations will be referred to as pseudorotations.[19]

Although the JT effect cannot result in a fullerene ion being observed in a reduced symmetry in general, a distorted geometry could be observed if measurements are made on a sufficiently short time scale. In various cubic systems undergoing an $E \otimes e$ JT effect, the time scale has been calculated to be the order of picoseconds.[19] For C_{60}^-, an estimate from electron paramagnetic resonance (EPR) data[20] suggests a time scale of the order of picoseconds, while estimates from the strength of the vibronic coupling[21–25] suggest a time scale of the order of femtoseconds. Although this is a rapid time scale, it does suggest that modern ultrafast spectroscopic techniques should be capable of detecting the pseudorotational motion and hence determining pseudorotational rates. Indeed, ultrafast pump-probe spectroscopy has already been successfully used to determine the rate at which C_{60} and C_{70} molecules reorient themselves in solution.[26,27] However, no data is available for the determination of pseudorotation rates in C_{60}^- ions. The rate at which pseudorotation occurs must depend on the shape of the lowest APES, which, in turn, will depend on the vibronic coupling parameters. Hence the determination of pseudorotation rates will give important information about the strength and nature of the underlying vibronic coupling.

According to Hückel molecular orbital theory, when an extra electron is added to the neutral C_{60} molecule it will occupy a molecular orbital of T_{1u} symmetry.[28] Group theory dictates that vibronic coupling may occur between this level and eight h_g vibrational modes plus two a_g vibrational modes. The coupling to the a_g modes is trivial and need not be considered further. Thus the vibronic coupling problem relevant to C_{60}^- ions is a $T_{1u} \otimes 8h_g$ JT problem.[8] For many purposes, it is sufficient to consider coupling to a single effective mode in the simpler $T_{1u} \otimes h_g$ JT problem,[29,30] although this works best when the JT coupling strengths and the spread in frequencies are rather less than those occurring in the fullerenes. Alternatively, theoretical results for coupling to all eight modes can be obtained explicitly.[8,31] In either case, it is necessary to know results for the single-mode $T_{1u} \otimes h_g$ JT problem. This is what we will consider here.

In this paper, we use the quantum mechanical time evolution operator to derive analytical expressions for the rates of pseudorotation in the $T_{1u} \otimes h_g$ coupling problem as a func-

tion of the vibronic coupling parameters. We will consider the situation in which quadratic coupling is present to warp the lowest APES to produce potential wells, although as mentioned above other perturbation effects produce essentially similar results. The results will apply for instances in which only the lowest vibronic levels play any significant role, and are therefore most appropriate to studies either at low absolute temperature or where the lowest vibronic levels are selected spectroscopically. Finally, as there is no pseudorotation data currently available on the C_{60}^- ion, we outline experiments that would be capable of determining such data. It is hoped that the results of these experiments on a series of ions derived from C_{60}, together with the theory given here, will be able to shed some light on the vibronic coupling in these very interesting and important ions.

II. THEORY

A. General theory of temporal evolution

In Ref. 19, it was shown how the temporal evolution of a system initially localized in a state $|w_i\rangle$ associated with a potential well can be followed using the usual time evolution operator

$$U_t(t) = \exp(-i\mathcal{H}t/\hbar), \tag{1}$$

where $\mathcal{H}$ is the JT Hamiltonian of the system. As the well states $|w_i\rangle$ are not eigenstates of the system due to tunneling between isoenergetic wells, it was therefore found more appropriate to express the result in terms of symmetry-adapted states $|\Gamma_i\rangle$ formed from linear combinations of the well states which reflect the correct symmetry of the problem (which is icosahedral in the current case). We will restrict our consideration to cases in which the oscillators associated with the wells are in their ground states. Therefore, if there are n isoenergetic wells, then there will be n symmetry-adapted ground states. Thus the n ground well states can be expressed as the linear combination

$$|w_i\rangle = \sum_{j=1}^{n} b_i^{(j)} |\Gamma_j\rangle \tag{2}$$

of symmetry-adapted ground states, where the $b_i^{(j)}$ are real constants.

The symmetry-adapted states are close approximations to the true eigenstates of the system, so we can write

$$\mathcal{H}|\Gamma_i\rangle = \mathcal{E}_i|\Gamma_i\rangle, \tag{3}$$

where $\mathcal{E}_i$ is the energy of the ith symmetry-adapted state $|\Gamma_i\rangle$. It thus follows that the temporal evolution of a well state $|w_i\rangle$ is given by

$$U_t|w_i\rangle = \sum_{j=1}^{n} b_i^{(j)} \exp(-i\mathcal{E}_j t/\hbar)|\Gamma_j\rangle. \tag{4}$$

An expression for the probability

$$P_{if} = |\langle w_f|U_t|w_i\rangle|^2 \tag{5}$$

that a system that starts off localized in an initial well $|w_i\rangle$ will have become localized in another well $|w_f\rangle$ a time t later, can then be calculated in terms of the $b_i^{(j)}$ and the so-called tunneling splittings, $\mathcal{E}_j - \mathcal{E}_k$, between the symmetry-adapted ground states. This allows the temporal development of a system initially localized in a particular well to be followed, and for the rates at which the system tunnels through the barriers between wells to be derived. The nature of this probability and its relation to the tunneling splittings will now be explored in detail for the $T_{1u} \otimes h_g$ system.

B. Theory for the $T_{1u} \otimes h_g$ system

We now require the general JT Hamiltonian for the $T_{1u} \otimes h_g$ system including linear and quadratic coupling. As the H representation occurs twice in the symmetric part of the Kronecker product $H \otimes H$, the general form for quadratic coupling is a linear combination of two distinct types of quadratic vibronic coupling. There is no unique way of specifying these two contributions. We will specify the form for the quadratic coupling using the Clebsch-Gordon coefficients as defined by Fowler and Ceulemans.[32] An explicit form for the Hamiltonian using these definitions was given in Ref. 18. The result is of the form

$$\mathcal{H} = \mathcal{H}_0 + \mathcal{H}_1(V_1, \mathbf{Q}) + \mathcal{H}_2^{(1)}(V_2, \mathbf{Q}^2) + \mathcal{H}_2^{(2)}(V_3, \mathbf{Q}^2), \tag{6}$$

where $\mathbf{Q}$ is a vector representing the normal-mode coordinates of the five components of the h_g mode of vibration. $\mathcal{H}_0$ is the uncoupled vibrational Hamiltonian describing the vibrations in the absence of vibronic coupling and $\mathcal{H}_1$ describes the linear interaction, characterized by the linear coupling parameter V_1. $\mathcal{H}_2^{(1)}$ and $\mathcal{H}_2^{(2)}$ describe the two types of quadratic interactions, characterized by quadratic coupling parameters V_2 and V_3, respectively. Here, we will find it useful to define dimensionless coupling parameters

$$V_1' = -V_1(\mu\hbar\omega^3)^{-1/2},$$

$$V_2' = V_2/\mu\omega^2,$$

$$V_3' = V_3/\mu\omega^2, \tag{7}$$

where μ is the mass of the h_g mode and ω is its frequency.

The relative values of the quadratic coupling parameters determine the actual shape of the APES. It can therefore be useful to define the quadratic coupling constants in terms of an overall magnitude v and a mixing angle β as

$$V_2' = v \sin\beta,$$

$$V_3' = v \cos\beta. \tag{8}$$

There are found to be either six pentagonal (D_{5d}) minima in the APES that depend upon the linear coupling constant V_1' and the quadratic constant V_2', or ten trigonal (D_{3d}) minima that depend upon V_1' and V_3'. More specifically, the D_{5d} points are minima and the D_{3d} points local maxima if $3V_2' > \sqrt{5}V_3'$ ($\tan\beta > \sqrt{5}/3$), as illustrated in Fig. 1(a), whereas if $3V_2' < \sqrt{5}V_3'$ ($\tan\beta < \sqrt{5}/3$) the D_{5d} points become local maxima and D_{3d} points minima, as illustrated in Fig. 1(b). Following the conventions used in Ref. 18, we have labeled

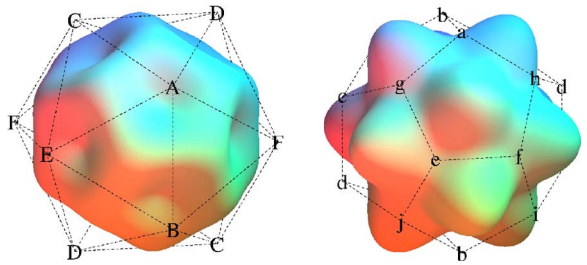

FIG. 1. (Color online) Representation of the two different kinds of warping of the APES of C_{60}^- due to the two different types of quadratic coupling. (a) The case when $V_1'=3$, $V_2'=0.5$, and $V_3'=0.05$, for which $3V_2'>\sqrt{5}V_3'$ and so pentagonal minima are created (labeled A, B, …), and (b) the case when $V_1'=3$, $V_2'=0.05$, and $V_3'=0.5$, for which $3V_2'<\sqrt{5}V_3'$ and the minima have trigonal symmetry (labeled a, b, …). The letters refer to the well labels used in Ref. 18.

the pentagonal wells using uppercase letters $A,B,\ldots,F$ and trigonal wells using lowercase letters $a,b,\ldots,j$. If $3V_2'=\sqrt{5}V_3'$ then the two terms "balance" and the APES takes the form of a spherical equal-energy surface, as is also the case when there is no quadratic coupling ($V_2'=V_3'=0$).

Reference 18 gave analytical expressions which can be taken as our well states $|w_i\rangle$ and symmetry-adapted states $|\Gamma_i\rangle$. When the D_{5d} points are minima, there are two triply degenerate states, with a T_{2u} tunneling state lying at an energy Δ above the T_{1u} ground state, as shown schematically in Fig. 2(a). Reference 18 gave expressions for the energies of the T_{1u} and T_{2u} states, from which an expression for Δ can be calculated to be

$$\Delta = -\frac{\hbar\omega S_p \ln S_p}{(1-S_p^2)}(2-\sqrt{2}V_2'+\sqrt{2/5}V_3') \tag{9}$$

where

$$S_p = \exp\left[-6\left(\frac{V_1'}{5-4\sqrt{2}V_2'}\right)^2\right] \tag{10}$$

is the phonon overlap between adjacent pentagonal wells. Δ is positive (and hence the T_{1u} state is the ground state) except for certain cases where the magnitude of one of the quadratic coupling constants is large compared to the linear coupling

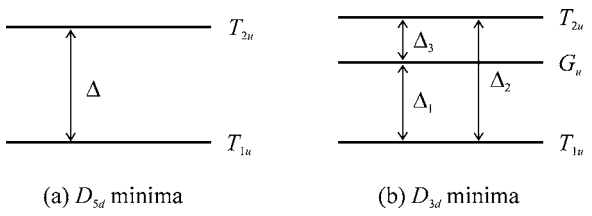

FIG. 2. Symmetry-adapted states formed by combining well states to give states with the correct symmetry. (a) The six D_{5d} wells combine to form a T_{2u} tunneling state an energy Δ above a T_{1u} ground state. (b) The ten D_{3d} wells combine to form tunneling states G_u and T_{2u} which lie at energies Δ_1 and Δ_2 above a T_{1u} ground state, respectively.

constant and the other quadratic coupling constant (so that $2-\sqrt{2}V_2'+\sqrt{2/5}V_3'<0$).

When the D_{3d} points are minima, there are tunneling states G_u and T_{2u} lying at energies Δ_1 and Δ_2 above the T_{1u} ground state, respectively (and hence separated by energy $\Delta_3=\Delta_2-\Delta_1$), as shown schematically in Fig. 2(b). From Ref. 18, we find that

$$\Delta_1 = -\frac{\hbar\omega S_t \ln S_t}{2(1-S_t^2)(3+2S_t)}(X+2S_tY),$$

$$\Delta_2 = -\frac{\hbar\omega S_t \ln S_t}{(1-S_t^2)(9-4S_t^2)}(3X-4S_t^2Y) \tag{11}$$

where

$$X = 10+\sqrt{2}V_2'-\sqrt{10}V_3',$$

$$Y = 5+2\sqrt{2}V_2'-\sqrt{10}V_3',$$

$$S_t = \exp\left[-12\left(\frac{V_1'}{3\sqrt{10}-8V_3'}\right)^2\right] \tag{12}$$

is the phonon overlap between adjacent trigonal wells. Again, the T_{1u} state is the ground state except for certain cases of one of the quadratic coupling constants being large. The ten trigonal wells divide such that any given well has a set of nearest neighbors and a set of next-nearest neighbors. The overlap between neighboring wells is S_t and that between next-nearest neighbors is S_t^2. It should be noted that the symmetry-adapted states are reasonable approximations to the true eigenfunctions of $\mathcal{H}$ in intermediate coupling, but are best in strong coupling where the minima are deeper.

III. RESULTS

The temporal evolution of a well state may now be followed using the method outlined in Sec. II A. We will consider the cases of pentagonal and trigonal minima in turn.

A. Pentagonal minima

If pentagonal wells are minima, we find that the probability that the system has migrated from well A to any adjacent well, say well B, during the interval t is given by

$$P_{AB}(t) = \frac{1}{5}[S_p^2+(1-S_p^2)\sin^2(\Delta t/2\hbar)] \tag{13}$$

and the probability that the system remains in well A is

$$P_{AA}(t) = 1-(1-S_p^2)\sin^2(\Delta t/2\hbar). \tag{14}$$

The sum of the probabilities of being in any of the six well states at time t is

$$\sum_{X=A}^{F} P_{AX} = 1+S_p^2. \tag{15}$$

The probability sum is independent of time, and tends to one in the infinite coupling limit. This is to be expected as the

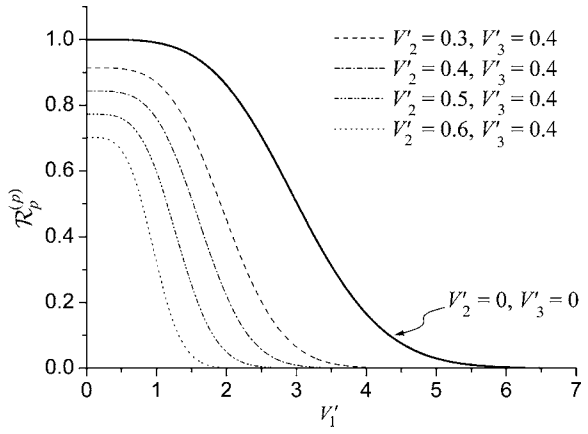

FIG. 3. Dimensionless pseudorotational rates $\mathcal{R}_p^{(p)}$ as a function of the dimensionless linear coupling constant V'_1 for the case of pentagonal minima. Various degrees of quadratic coupling are shown illustrating the effect of increasing V'_2 (V'_3 has a fixed, arbitrary value of 0.4). The solid line shows the situation in the absence of quadratic coupling.

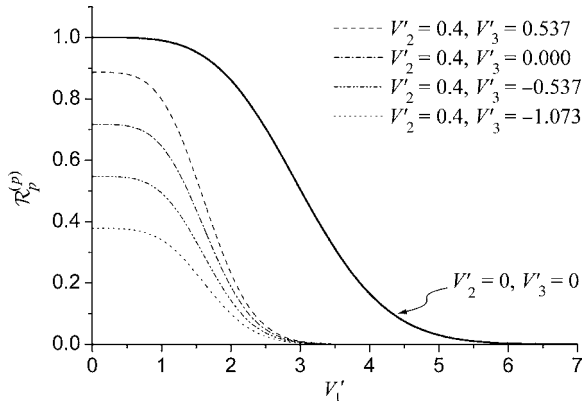

FIG. 4. As Fig. 3, but illustrating the effect of varying V'_3. V'_2 has been given an arbitrary value of 0.4 and V'_3 has been taken to be multiples of the maximum value ($3V'_2/\sqrt{5} \approx 0.537$) required to produce pentagonal wells.

system must be localized in one of the wells. The sum is greater than one in finite coupling. This is because of the spatial extent of the wave functions, as discussed in Ref. 19 in the context of the $E \otimes e$ problem. For example, even if the system has the highest probability of being in well state $|A\rangle$ at a given time, there is a finite probability of the system actually being found in one of the other wells at this time.

The simple $\sin^2$ dynamics indicated by Eqs. (13) and (14) may have been anticipated by analogy to the $E \otimes e$ system (as seen in Fig. 2 of Ref. 19), even though we now have six wells rather than three. In both systems, there is one tunneling level. As in the $E \otimes e$ case, we can define a pseudorotational period $T_p^{(p)}$ as the time taken to complete a complete circuit of the wells [where the superscript (p) indicates pseudorotation amongst pentagonal minima]. We can see that this occurs when the argument inside the $\sin^2$ factor in Eq. (14) increments by π, namely when

$$T_p^{(p)} = \frac{2\pi\hbar}{|\Delta|}. \tag{16}$$

We can then also define a pseudorotational rate $R_p^{(p)}$ as $R_p^{(p)} = 1/T_p^{(p)}$. It is also convenient to define a dimensionless pseudorotation rate

$$\mathcal{R}_p^{(p)} = 2\pi R_p^{(p)}/\omega = |\Delta|/\hbar\,\omega. \tag{17}$$

Representative plots of the dimensionless pseudorotational rate are shown in Figs. 3 and 4. The permitted values of V'_2 lie in the range $\sqrt{5}V'_3/3 < V'_2 < 5/4\sqrt{2}$. The upper limit corresponds to infinitely deep potential wells [i.e., when the denominator in the exponential in Eq. (10) becomes zero] and the lower limit is the condition to ensure pentagonal wells. Figure 3 shows that an increase in V'_2 (with fixed V'_3) causes a decrease in the pseudorotation rate, which occurs because increasing V'_2 increases the warping of the APES and makes propagation between wells more difficult. For a given V'_2, Fig. 4 shows that the pseudorotational rate also decreases for a decrease in V'_3. In the limit as $\sqrt{5}V'_3 \to 3V'_2$, the APES regains spherical symmetry and pseudorotation between wells will be its fastest. Decreasing V'_3 below this limit therefore increases warping and reduces the rate of pseudorotation.

$T_p^{(p)}$ corresponds to the time taken for the system to pseudorotate one complete "circuit" of the pentagonal wells. The average time taken to migrate from one given well to another, i.e., the time at which P_{AB} peaks (which can be interpreted as allowing for all possible paths), will be $T_p^{(p)}/2$. It is then useful to associate a tunneling time with the extra time taken to move from well to well due to warping of the APES compared to the time taken to pseudorotate around a trough in the linear problem. A similar approach was used in the $E \otimes e$ problem.[19] This time can be written as

$$\tau_t^{(p)} = \frac{1}{2}[T_p^{(p)} - f_{ref}^{(p)}], \tag{18}$$

where $f_{ref}^{(p)}$ is a reference function chosen so that $\tau_t^{(p)}$ vanishes in the absence of warping. Unfortunately, as the warping depends on both V'_2 and V'_3 there is no obvious way of defining this function. This is in contrast to the $E \otimes e$ case where warping only depends on one quadratic coupling parameter and can be "turned off" by setting this parameter to zero. For our purposes here, we take our reference function to be $T_p^{(p)}$ for the specific case of $V'_3 = 3V'_2/\sqrt{5}$. This choice is made because warping vanishes in the limit as $V'_3 \to 3V'_2/\sqrt{5}$ and, because S_p does not depend on V'_3, it allows a simple expression for the tunneling time to be formulated. The tunneling rate $R_t^{(p)} = 1/\tau_t^{(p)}$ and dimensionless tunneling rate $\mathcal{R}_t^{(p)} = 2\pi R_t^{(p)}/\omega$ can then be derived from the tunneling time. The latter takes the form

$$\mathcal{R}_t^{(p)} = \frac{2\sqrt{2}(5 - \sqrt{2}V'_2)\left(2 - \sqrt{2}V'_2 + \sqrt{\frac{2}{5}}V'_3\right)S_p \ln S_p}{(\sqrt{5}V'_3 - 3V'_2)(1 - S_p^2)}. \tag{19}$$

Assuming a representative value of $V'_1 = 3$, we can plot $\mathcal{R}_t^{(p)}$ as a function of the quadratic coupling constants, as shown in

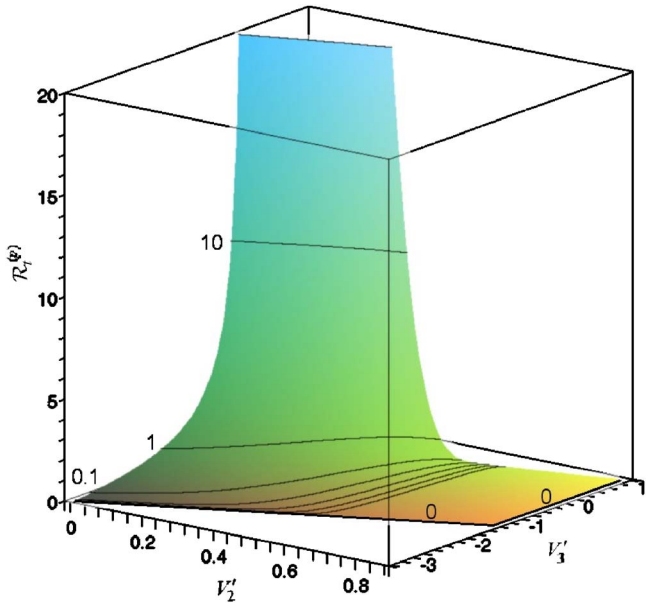

FIG. 5. (Color online) A surface plot of the dimensionless tunneling rate $\mathcal{R}_t^{(p)}$ as a function of the (dimensionless) quadratic coupling constants. The linear parameter has been taken to be $V_1'=3$. The contours show the behavior for $\mathcal{R}_t^{(p)}=10,1,0.1,\ldots$, i.e., values decreasing tenfold each time. The lines labeled "0" represent the limit of this progression where $\mathcal{R}_t^{(p)}=0$.

Fig. 5. If we consider some point on this surface, then we see that increasing V_2' or decreasing V_3' reduces the tunneling rate. This occurs because these changes lead to the APES becoming progressively more warped. On the other hand, decreasing V_2' reduces warping so that the tunneling rate increases and approaches a finite limiting value if $V_3'<0$. If $V_3'\geq 0$, $\mathcal{R}_t^{(p)}$ increases without limit as we tend to a situation in which the APES becomes spherically symmetric and so the extra time to "tunnel" (rather than pseudorotate) becomes vanishingly small. Similarly, increasing V_3' for any initial position will tend to this same unwarped scenario and so an infinite rate. Thus, the tunneling rate defined in Eq. (18), when used with the proposed reference function, behaves in a manner that seems entirely reasonable.

B. Trigonal minima

If trigonal wells are minima, the situation is somewhat more complicated than for the pentagonal wells and the $E\otimes e$ case,[19] where there was one tunneling splitting and migration to another well followed a simple temporal pattern because all the wells to which the system can migrate are equivalent. For the trigonal wells, there are two different tunneling splittings involved and we need to consider the possibility that the system has migrated to either a nearest-neighbor well or a next-nearest-neighbor well. If we start off in well a, then, as can be seen in Fig. 1(b), we need to find the probability that the system has evolved to either one of the equivalent sets of nearest-neighbor wells $\{b,g,h\}$ or to one of the set of next-nearest-neighbors $\{c,d,e,f,i,j\}$. Using the results in Ref. 18 we find that the probabilities of finding

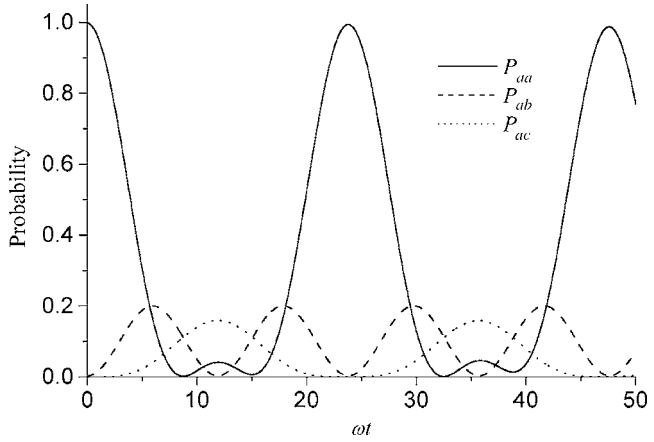

FIG. 6. Probability plots showing the variation of P_{aa}, P_{ab}, and P_{ac} as a function of ωt. The vibronic coupling constants have been taken as $V_1'=3$, $V_2'=0.1$, and $V_3'=0.4$ ($S_t\approx 0.0651$).

a system initially in well a in the same well a, a nearest-neighbor well (e.g., b) or a next-nearest-neighbor well (e.g., c) respectively, at a time t later are

$$P_{aa}(t)=1-\frac{1}{25}(1-S_t^2)(4S_1+S_2),$$

$$P_{ab}(t)=\frac{5}{9}S_t^2+\frac{1}{45}(1-S_t^2)S_2,$$

$$P_{ac}(t)=\frac{1}{9}S_t^4+\frac{1}{225}(1-S_t^2)(6S_1-S_2), \tag{20}$$

where

$$S_1=(3+2S_t)(1+S_t)\sin^2\frac{\Delta_1 t}{2\hbar}+(3-2S_t)(1-S_t)\sin^2\frac{\Delta_3 t}{2\hbar},$$

$$S_2=(9-4S_t^2)\sin^2\frac{\Delta_2 t}{2\hbar}. \tag{21}$$

The sum of the probabilities of a system initially in well a being found in any well at time t is given by

$$\sum_{x=a}^{j}P_{ax}(t)=\frac{1}{3}(3+2S_t^2)(1+S_t^2), \tag{22}$$

which is independent of time as in the previous cases. However, the interwell dynamics are otherwise clearly more complicated in this trigonal case. The differences are most clearly seen when we plot the variations in probabilities given in Eqs. (20). The variation for small times is illustrated in Fig. 6. Initially, the system is localized in well a, and therefore the probabilities of finding the system in wells b and c are very small (but not zero, due to the spatial extent of the wave function). With time, the system evolves so that the probability that the system is still localized in well a decreases and the probabilities of finding it in well b or well c start to increase. The rate of increase in P_{ac} is smaller than P_{ab}, meaning that the system is more likely to be in well b than c.

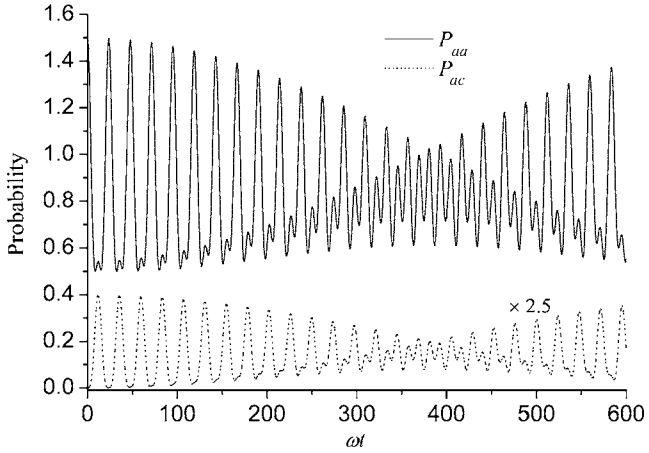

FIG. 7. Probability plots showing the long-term variation of P_{aa} and P_{ac} as a function of ωt. The vibronic coupling constants have again been taken as $V_1'=3$, $V_2'=0.1$, and $V_3'=0.4$ ($S_t \approx 0.0651$). For clarity, the P_{aa} data has been offset by 0.5 and that for P_{ac} has been scaled by a factor of 2.5.

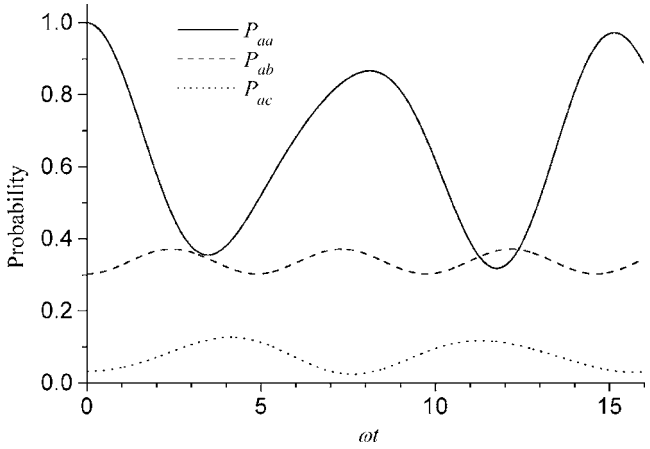

FIG. 8. Probability plots showing the interwell dynamics in the presence of weak linear vibronic coupling. The actual parameters used are $V_1'=1$, $V_2'=0.1$, and $V_3'=0.4$ ($S_t \approx 0.738$).

This is expected as well b is a nearest-neighbor well and c is a next-nearest-neighbor. As time progresses, the system becomes increasingly more likely to be found in well b, and then well c.

The values of the probability maxima can also be understood. As the system evolves out of well a, it can migrate to any of the equivalent wells $\{b,g,h\}$ with equal probability. The maximum in $P_{ab} \sim 0.2$ is therefore much smaller than the value of unity observed for P_{aa}. A similar decrease in maximal probability is observed as the system evolves into a combination of the six equivalent wells $\{c,d,e,f,i,j\}$.

Figure 6 shows the system starting in well a, moving through wells $\{b,g,h\}$, then through wells $\{c,d,e,f,i,j\}$, back through wells $\{b,g,h\}$, and finally back to well a. This process of evolution then repeats itself. However, the state after one round trip is not identical to the initial state. It is difficult to see this in Fig. 6, but it becomes more apparent if the process is followed over an extended period of time as in Fig. 7, which shows the same plots of P_{aa} and P_{ac} as in Fig. 6 but displayed over a longer period of time. The observed behavior occurs because, while P_{ab} contains a single $\sin^2$ term, P_{aa} and P_{ac} contain three $\sin^2$ terms with different periods. The overall effect is that whenever a "reoccurrence" of the initial state happens, an increasingly larger proportion of the system gets "left behind" in the wells $\{c,d,e,f,i,j\}$.

In Eq. (16), we were able to formulate an expression for the pseudorotation time $T_p^{(p)}$ in the D_{5d} case for a complete circuit of distortion. The complicated dynamics in the D_{3d} case makes it difficult to formulate a closed analytical expression for an equivalent rate of pseudorotation $T_p^{(t)}$ here. An accurate value can be calculated numerically for any chosen set of vibronic coupling parameters by finding the times at which $\partial P_{aa}/\partial t=0$. This has been done using a simple Newton-Raphson procedure, checking that the root obtained converges to the appropriate stationary point. However, it is possible to deduce an approximate analytical formula by examining Eq. (11). From these expressions, it is apparent that in the strong-coupling limit, $S_t \to 0$ and $\Delta_2/\Delta_1 \to 2$. We can then see from Eqs. (20) that $T_p^{(t)}=2\pi\hbar/|\Delta_1|=4\pi\hbar/|\Delta_2|$ is the exact time required to undergo one complete circuit from well a and back to well a. Also, Fig. 6 shows that, for the specific values of the vibronic constants used in the plot, the time taken for one circuit from well a to well a is approximately four times the time taken for the system to migrate to well b. This suggests a suitable definition of the pseudorotational period here would be $T_p^{(t)} \approx 4\pi\hbar/|\Delta_2|$. However, this plot is for strong linear coupling. If we reduce the value of the linear coupling parameter (so that S_t is no longer small, but may approach unity) and reexamine the interwell dynamics, this approximation is seen to fail. An illustrative case is shown in Fig. 8. In fact, the pseudorotation period in this example (i.e., the time taken to return to well a) is more closely represented by $T_p^{(t)} \approx 2\pi\hbar/|\Delta_1|$. Once again, inspection of Eqs. (20) is helpful. In the limit as $\Delta_2/\Delta_1 \to 1$, these expressions show that the time taken for the system to evolve back to well a is exactly equal to $2\pi\hbar/|\Delta_1|$. In the limit as $S_t \to 1$, Eq. (11) indicates that $\Delta_2/\Delta_1 \approx 1$ providing V_2' and V_3' are small. Hence the approximate pseudorotation period $T_p^{(t)} \approx 2\pi\hbar/|\Delta_1|$ becomes appropriate in the limit of weak vibronic coupling where $S_t \approx 1$, as in Fig. 8.

It seems entirely reasonable that the pseudorotation period should in general depend on the two tunneling splittings observed. Therefore, somewhat heuristically, we define the pseudorotation period in the case of trigonal minima as

$$T_p^{(t)} = \frac{2\pi\hbar}{|\Delta_1|} S_t + \frac{4\pi\hbar}{|\Delta_2|}(1-S_t). \tag{23}$$

The validity of this expression can then be checked against the numerical results for some specific sets of coupling constants. As can be seen in Table I, the approximate expression for the pseudorotation period is highly accurate provided the coupling constants are sufficiently large.

The validity of this expression can then be checked against the numerical results for some specific sets of coupling constants. As can be seen in Table I, the approximate expression for the pseudorotation period is highly accurate provided the coupling constants are sufficiently large. The

TABLE I. Pseudorotation periods $\omega T_p^{(t)}$ in the presence of trigonal minima. Vibronic coupling parameters have been chosen to highlight errors between the approximate expression [Eq. (23)] and true values obtained numerically by finding the appropriate root of $\partial P_{aa}/\partial t=0$.

Coupling constants			$\omega T_p^{(t)}$			
V_1'	V_2'	V_3'	S_t	True value	Equation (23)	Percent error
1	0.1	0.4	0.738	8.115	8.245	1.6
3	0.1	0.4	0.065	23.79	23.78	2.3×10^{-2}
5	0.1	0.4	0.0005	1107	1107	1.5×10^{-6}
0.1	0.1	0.3	0.998	6.917	7.049	1.9
0.1	0.1	0.4	0.997	7.247	7.445	2.7
0.1	0.1	0.5	0.996	7.688	7.888	2.6
0.1	0.1	0.6	0.995	8.366	8.387	0.25
0.1	0.2	0.6	0.995	7.793	8.017	2.9
0.1	0.3	0.6	0.995	7.486	7.680	2.6
0.1	0.4	0.6	0.995	7.276	7.372	1.3
0.1	0	1.134	0.5	12.66	13.05	3.0
0.8	0	0.770	0.5	10.78	10.77	0.11
1.6	0	0.354	0.5	9.126	9.040	0.94
2.2	0	0.0416	0.5	8.106	8.088	0.23

form of Eq. (23) suggests that the largest errors should occur when $S_t \simeq 0.5$. To investigate this, we show in Table I some representative calculations in which we choose coupling parameters so that $S_t=0.5$. The errors are again seen to be quite small. Larger, errors are possible if very shallow wells are considered, for example, $V_1'=1.6$, $V_2'=0$, and $V_3'=0.01$ ($S_t \simeq 0.707$) results in an error of 12%. However, in these cases the theory, which depends on the combination of wells, is not expected to give a good account of the vibronic coupling. In what follows, we shall use Eq. (23) to explore the pseudorotational behavior as a function of the coupling parameters. However, interpretation of real pseudorotational data would best be approached using the accurate expressions given in Eq. (20).

A trivial, but interesting, application of Eq. (23) is the calculation of the relative rates of pseudorotation for the two cases illustrated in Fig. 1. Using Eq. (23), the pseudorotation period in the strongly coupled case with V_3' strongest shown in Fig. 1(b) is calculated to be $T_p^{(t)}=44.70/\omega$. In Fig. 1(a), the coupling is also strong but favors the V_2'-type of quadratic coupling. Here, Eq. (16) leads to $T_p^{(p)}=38940/\omega$. Thus the relative rates of pseudorotation will be $T_p^{(p)}/T_p^{(t)} \approx 870$. That is, for the same degrees of quadratic vibronic coupling but of the opposite types, pseudorotation will be much faster if the V_3'-type of coupling dominates ($V_3'/V_2' \gg 1$). In other words, as a general rule, the presence of trigonal minima will favor faster pseudorotation. This is what would be expected from a consideration of the barriers to pseudorotation implied in Fig. 1.

As in the previous cases, Eq. (23) gives pseudorotation rates and dimensionless pseudorotation rates in the presence of trigonal minima of

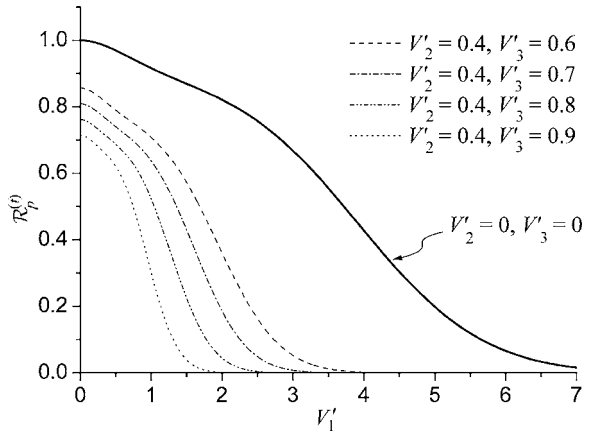

FIG. 9. Dimensionless pseudorotational rates $\mathcal{R}_p^{(t)}$ as a function of the dimensionless linear coupling constant V_1' for the case of trigonal minima. Various degrees of quadratic coupling are shown illustrating the effect of increasing V_3' (the other quadratic constant has been fixed at $V_2'=0.4$). The solid line shows the situation in the absence of quadratic coupling.

$$R_p^{(t)} = 1/T_p^{(t)},$$

$$\mathcal{R}_p^{(t)} = \frac{2\pi R_p^{(t)}}{\omega} = \left[\frac{S_t}{|\Delta_1|/\hbar\,\omega} + \frac{2(1-S_t)}{|\Delta_2|/\hbar\,\omega}\right]^{-1}. \qquad (24)$$

Figures 9 and 10 show plots of the dimensionless pseudorotation rate for various degrees of vibronic coupling. As can be seen in the figures, an increase in V_3' causes a decrease in pseudorotation rate. This is because V_3' is now the primary warping mechanism, so that an increase in its value increases warping making it more difficult to progress between wells. On the other hand, V_2' has a maximum value determined by the condition $3V_2' < \sqrt{5}V_3'$, the upper limit corresponding to a smooth, unwarped, APES. Lowering V_2' below this limit increases warping and therefore decreases the pseudorotation rate. Thus the roles of V_2' and V_3' have been reversed compared to the case of pentagonal wells.

In a real system exhibiting $T_{1u}\otimes h_g$ vibronic coupling, both types of quadratic coupling will be present ($V_2' \neq 0, V_3' \neq 0$). However, it is interesting to consider how these two

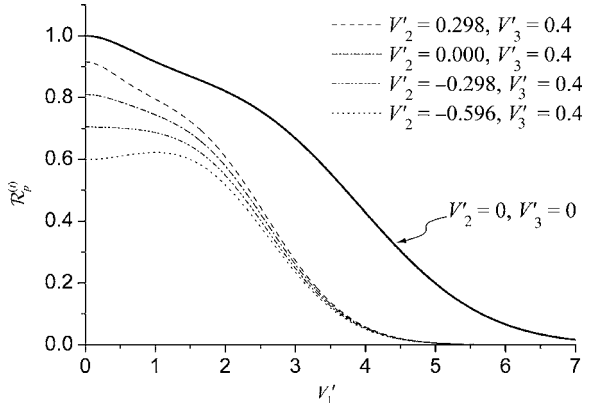

FIG. 10. As Fig. 9, but illustrating the effect of varying V_2'. V_3' has been arbitrarily set at 0.4 and V_2' taken to be multiples of its maximum permissible value $\sqrt{5}V_3'/3 \approx 0.298$.

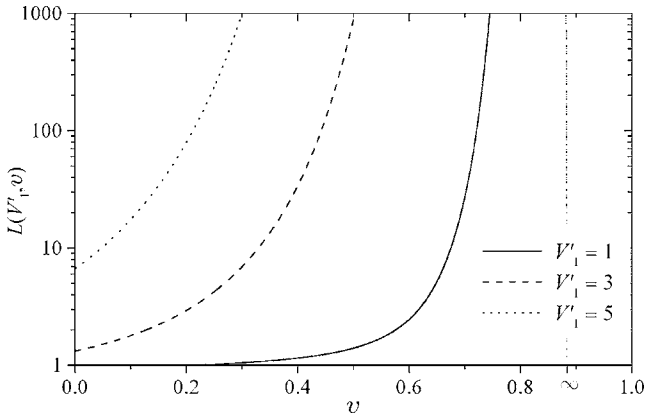

FIG. 11. The variation of $L(V'_1,v)$ with quadratic coupling parameter v for several values of the linear coupling parameter V'_1. The broken line labeled ∞ marks the limit where $L\to\infty$, and a logarithmic scale is used on the vertical axis for the sake of clarity.

independent types of quadratic coupling coefficients each separately affect the pseudorotation rate. More specifically, for a certain degree of quadratic coupling v we will compare the rate at which pseudorotation occurs when there is only one type of quadratic coupling present, i.e., we will compare $\mathcal{R}_p^{(t)} \equiv \mathcal{R}_p^{(t)}(V'_1,V'_2,V'_3)$ with V'_2 set to zero and $\mathcal{R}_p^{(p)} \equiv \mathcal{R}_p^{(p)}(V'_1,V'_2,V'_3)$ with V'_3 set to zero. Thus, we define

$$L(V'_1,v) = \frac{\mathcal{R}_p^{(t)}(V'_1,0,v)}{\mathcal{R}_p^{(p)}(V'_1,v,0)}. \tag{25}$$

Figure 11 shows plots of this function for various degrees of linear and quadratic coupling. It is seen that for identical quadratic coupling strengths the pseudorotation rate is always faster in the presence of trigonal minima. Furthermore, the pseudorotation between trigonal wells can be orders of magnitude greater than that between pentagonal wells provided the linear or quadratic coupling strengths are sufficiently large. As already mentioned, this is perhaps not too surprising in view of the general shapes of the APESs as depicted in Fig. 1.

As with pentagonal wells, if the trigonal wells are sufficiently deep, the system must tunnel between equivalent minima, taking an additional time $\tau_t^{(t)}$ over that required for a simple pseudorotation. However, in this case, there is the added complication that a system initially localized in one minimum can tunnel to two different types of available minima. For simplicity, we consider here only the rate of tunneling to an adjacent minimum. This is justified because tunneling will only occur when the minima are sufficiently deep. Under these conditions, the rate at which the system tunnels to one of the next-nearest minima is likely to be much smaller than the rate at which it tunnels to a nearest neighbor. However, should a rate for tunneling to next-nearest neighbors be required, it can easily be calculated using an obvious extension of the theory used here.

In order to calculate the rate at which the system tunnels from one trigonal well to an adjacent well, we need to reexamine the time-dependent probabilities in Eqs. (20). In particular, we see from P_{ab} that the time taken to migrate to an adjacent well is represented by $\pi\hbar/|\Delta_2|$. Using the same arguments as before, we take our reference time to be $\pi\hbar/|\Delta_2|$ for the case when $V'_2=\sqrt{5}V'_3/3$ so that the tunneling rate is given by

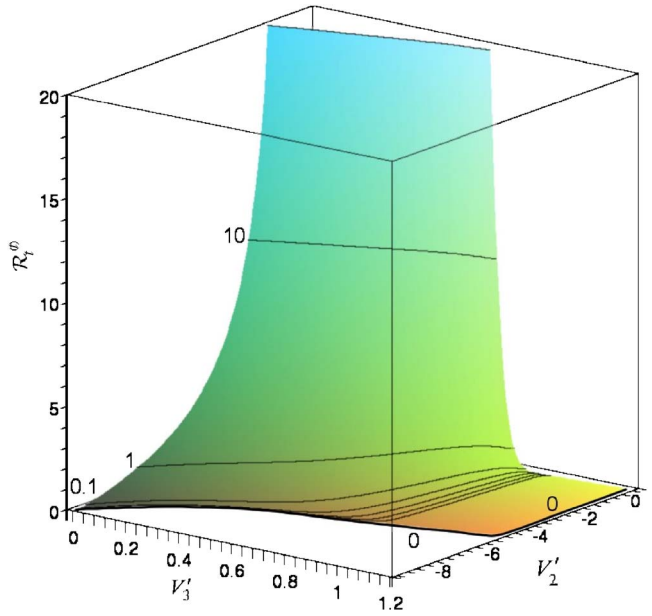

FIG. 12. (Color online) Plot of the dimensionless tunneling rate $\mathcal{R}_t^{(t)}$. The linear coupling parameter has again been taken to be $V'_1=3$, and the contours vary logarithmically (cf. Fig. 5).

$$R_t^{(t)} = \left[\frac{\pi\hbar}{|\Delta_2|} - \frac{\pi\hbar}{|\Delta_2^{ref}|}\right]^{-1}, \tag{26}$$

where $|\Delta_2^{ref}|$ is the value of $|\Delta_2|$ with $V'_2=\sqrt{5}V'_3/3$. Once again, $R_t^{(t)}$ will be converted into a dimensionless tunneling rate $\mathcal{R}_t^{(t)}=2\pi R_t^{(t)}/\omega$. Figure 12 shows a plot of this function for the case when the dimensionless linear coupling parameter has the value $V'_1=3$. This figure can be compared to the equivalent plot for tunneling between pentagonal wells in Fig. 5. The two figures are very similar, which suggests that the tunneling rates in the two different cases are broadly the same. However, these figures illustrate only one particular value of V'_1, and also do not permit a clear comparison of the rates of tunneling in the two different cases.

IV. DISCUSSION

To our knowledge, there have been no experiments reported to date that quantify pseudorotation in JT-active derivatives of C_{60}. We expect pseudorotation to be faster than molecular rotation, which itself occurs on a time scale of a few picoseconds. Detection of rates down to a few femtoseconds should be possible in ultrafast optical experiments. Clearly, such experiments would give valuable information about vibronic interactions in these systems. Equally clearly, it is apparent that interpretation of pseudorotational dynamics in these systems will be a nontrivial exercise. In this section, we outline experiments that should be able to detect pseudorotation in ionic derivatives of C_{60}. Furthermore, it is

hoped that such experiments may be able to be used to measure pseudorotation rates and thereby reveal useful information concerning the linear and quadratic coupling constants in these ions.

A. Reorientational dynamics of neutral C_{60}

The rotational motion of molecules in liquids is of interest because it plays a role in determining the efficiency and outcome of chemical reactions in solution. Also, such studies give information on a molecular scale of various interesting phenomena, such as solute-solvent interactions and diffusion. One method of monitoring rotation in liquids is via the so-called "transient grating" technique. These experiments involve pumping the sample of interest with two ultrafast laser pulses to produce a disturbance within the sample with the characteristics of a diffraction grating. A weak probe beam is then applied which responds to the diffraction grating and thus allows monitoring of the grating itself. With time, the grating degrades via several decay mechanisms and this can be monitored by changing the time delay between the pumps and the probe beams. Using this technique, the decay of the grating due to molecular reorientation can be determined. Now, it must be expected that experiments that can in some sense follow the rotation of molecules in solution should also be able to detect pseudorotation in suitably active JT systems. Therefore the rotational reorientational dynamics of fullerene molecules and ions in solution should provide interesting and potentially quantitative data on pseudorotation and vibronic interactions in these systems.

Reorientation studies on C_{60} and C_{70} have been carried out using a four-wave mixing (FWM) technique.[26,27] Not surprisingly, these studies reveal that the reorientation rate is strongly dependent on the solvent used. It is interesting here to compare the reorientation of C_{60} and C_{70} in the same solvent. As shown in Fig. 13, the transient signal resulting from the two molecules are quite distinct. For C_{60}, the signal amplitude is found to decay exponentially, whereas a biexponential decay is observed for C_{70}.

The different reorientational dynamics for these molecules is attributable to their different geometries. In C_{60}, all atoms lie on a spherical shell whose center coincides with the center of the molecule. Therefore as this molecule reorients itself rotation in any direction is equivalent, leading to a single decay rate. However, the C_{70} molecule is not spherical. An arbitrarily oriented molecule will therefore present to the reference direction, defined by the polarization of the pump beams, two types of rotational reorientation. Around the long axis of the molecule the rotation is expected to be very similar to that in C_{60}, as is observed (time τ_1). On the other hand, rotation around a short axis will be slower as this rotation will incur more resistance from the surrounding solvent molecules (τ_2). It is important to note that the C_{60} and C_{70} molecules have a very similar appearance but the differences in their rotational dynamics are readily observable using the FWM technique.

Transient grating experiments should be sensitive to pseudorotation because pseudorotation in the sample molecules will present itself as another decay mechanism to the transient grating. This "pseudo-reorientation" mechanism should be experimentally observable in samples of JT-active fullerene derivatives and should, therefore, provide access to useful information on the JT interactions in such systems.

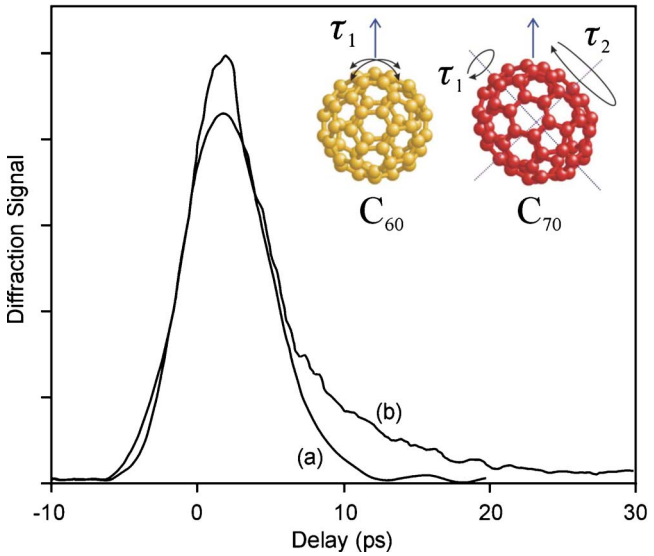

FIG. 13. (Color online) Transient four-wave mixing signals from solutions of (a) C_{60} and (b) C_{70} in chlorobenzene (adapted from Ref. 27). The inset depicts reorientation in C_{60} and C_{70}. Due to its higher symmetry, reorientation in C_{60} is simpler than in C_{70}, and requires only one parameter, τ_1. In C_{70}, reorientation can also occur around the short axis of the molecule, which requires an additional reorientational parameter τ_2. The vertical arrows denote the direction defined by the polarization of the pump lasers.

B. Pseudo-reorientation in C_{60} ions

As already discussed, four-wave mixing experiments[26] on neutral C_{60} in solution give information on the reorientation dynamics of the neutral molecule. This molecule is not subject to the JT effect in the ground state and so one would not expect to see strong pseudorotational signatures in the FWM signal. However, if the same experiment was repeated using one of the anions C_{60}^{-},C_{60}^{2-}, …, or one of the cations C_{60}^{+}, C_{60}^{2+}, …, one would expect to observe signals exhibiting characteristics attributable to pseudorotation. On a femtosecond time scale a C_{60}^{-} ion, for example, will not exhibit icosahedral symmetry but will be distorted. Therefore the FWM signal may become biexponential, as observed for C_{70} (Fig. 13). Also, as with the Na_3 molecule, one might expect to observe oscillations in the signal which will give a strong indication of the actual vibrational modes involved in the pseudorotation. However, the precise nature of the way in which the dynamical aspects of the JT effect become manifest in these ions awaits experimental determination.

Carrying out such experiments in solution has some noteworthy advantages and disadvantages. One disadvantage is that there is the complication of solvent effects to consider. This is not likely to alter the overall picture of the pseudorotation, although any solvent-dependent differences in the coupling constants will lead to different pseudo-reorientation rates. We note, however, that pseudo-reorientation may be

less dependent on the solvent than proper reorientation. This is because a proper rotation involves movement of the nuclei around the center of the molecule and thus requires a great deal of interaction with the solvent molecules. During pseudorotation, however, the nuclei move by small amounts towards or away from the center of the molecule and, as long as a set of equivalent distorted configurations are still available, this should incur much less resistance from the solvent. This insensitivity to solvent may prove advantageous in helping to identify pseudorotational effects, with any differences between solvents providing information on the role of the solvents.

Another advantage of carrying out experiments in solution is that it has been found that it is relatively easy to electrochemically add up to six electrons to C_{60}.[33] Therefore, one can perform FWM and, perhaps, other nonlinear experiments on a series of JT active ions using the same solvent and making very little change to the fullerene ion apart from the oxidation state. This will minimize cross-solvent interference and allow easy comparison of the dynamics in a wide range of fullerene ions. Yet another advantage is that it is relatively easy to perform experiments in solution at thermostatically controlled temperatures. The rate of pseudorotation should be strongly temperature dependent because higher temperatures will lead to population of excited vibronic states wherein pseudorotation is inherently faster. The additional information arising from a series of experiments at different temperatures may, therefore, be useful in extracting information on the quadratic vibronic coupling in these ions.

V. SUMMARY AND CONCLUSIONS

In this work, we have derived analytical expressions for pseudorotation rates in the $T_{1u} \otimes h_g$ JT system. We have shown that the dynamics is relatively simple when there are minima of D_{5d} symmetry in the APES, but rather more complicated when the minima are of D_{3d} symmetry. This is due to the more complicated tunneling splittings between the symmetry-adapted states that correctly describe tunneling between equivalent minima. One consequence of this is that observation of interwell dynamics in a real $T_{1u} \otimes h_g$ system, such as in the C_{60}^- ion, would allow unequivocal determination of the nature of the minima in the APES.

The method as presented here does not include the effect of excited vibronic states. However, the theory could be extended in this manner to permit the effect of temperature variation on the rate of pseudorotation to be accounted for. This in turn may be used to investigate high order vibronic coupling effects in real systems.

Ultrafast optical experiments have already been used to observe pseudorotation in some simple $E \otimes e$ systems. For the fullerene ions, no such data is available. We have outlined experiments that should be capable of measuring pseudorotation in these ions using transient grating techniques. To date, we are unsure of the exact nature of the pseudorotational signatures that might be forthcoming. However, what can be expected is that if pseudorotation in these ions can be identified and measured, then new information concerning vibronic interactions in these fullerenes would be forthcoming.

ACKNOWLEDGMENT

We thank EPSRC (UK) for providing funds for this work.

*Electronic address: janette.dunn@nottingham.ac.uk; URL: http://www.nottingham.ac.uk/~ppzjld

[1] M. S. Dresselhaus, G. Dresselhaus, and P. C. Eklund, *Science of Fullerenes and Carbon Nanotubes* (Academic Press, San Diego, 1996).
[2] S. Margadonna and K. Prassides, J. Solid State Chem. **168**, 639 (2002).
[3] O. Gunnarsson, Rev. Mod. Phys. **69**, 575 (1997).
[4] L. Forró and L. Mihály, Rep. Prog. Phys. **64**, 649 (2001).
[5] R. Moret, Acta Crystallogr., Sect. A: Found. Crystallogr. **61**, 62 (2005).
[6] D. Arčon and R. Blinc, Struct. Bond. **109**, 231 (2004).
[7] V. Brouet, H. Alloul, S. Gàràj, and L. Forrò, Struct. Bond. **109**, 165 (2004).
[8] C. C. Chancey and M. C. M. O'Brien, *The Jahn-Teller Effect in C_{60} and Other Icosahedral Complexes* (Princeton University Press, Princeton, 1997).
[9] M. C. M. O'Brien, Phys. Rev. B **53**, 3775 (1996).
[10] J. L. Dunn, M. R. Eccles, Y. Liu, and C. A. Bates, Phys. Rev. B **65**, 115107 (2002).
[11] F. S. Ham, in *Electron Paramagnetic Resonance*, edited by S. Geschwind (Plenum, New York, 1972), pp. 1–119.
[12] I. B. Bersuker and V. Z. Polinger, *Vibronic Interactions in Molecules and Crystals* (Springer, Berlin, 1989).
[13] U. Öpik and M. H. L. Pryce, Proc. R. Soc. London, Ser. A **238**, 425 (1957).
[14] M. C. M. O'Brien, Proc. R. Soc. London, Ser. A **281**, 323 (1964).
[15] H. Bill, in *The Dynamical Jahn-Teller Effect in Localised Systems*, edited by Y. E. Perlin and M. Wagner (Elsevier, Amsterdam, 1984).
[16] M. Gerloch, Inorg. Chem. **20**, 638 (1981).
[17] R. J. Deeth and M. A. Hitchman, Inorg. Chem. **25**, 1225 (1986).
[18] J. L. Dunn and C. A. Bates, Phys. Rev. B **52**, 5996 (1995).
[19] I. D. Hands, J. L. Dunn, and C. A. Bates, Phys. Rev. B **73**, 014303 (2006).
[20] W. Z. Wang, C. L. Wang, A. R. Bishop, L. Yu, and Z. B. Su, Synth. Met. **86**, 2365 (1997).
[21] C. M. Varma, J. Zaanen, and K. Raghavachari, Science **254**, 989 (1991).
[22] N. Breda, R. A. Broglia, G. Colo, H. E. Roman, F. Alasia, G. Onida, V. Ponomarev, and E. Vigezzi, Chem. Phys. Lett. **286**, 350 (1998).
[23] O. Gunnarsson, H. Handschuh, P. S. Bechthold, B. Kessler, G. Gantefor, and W. Eberhardt, Phys. Rev. Lett. **74**, 1875 (1995).
[24] A. S. Alexandrov and V. V. Kabanov, Pis'ma Zh. Eksp. Teor. Fiz. **62**, 920 (1995) [JETP Lett. **62**, 937 (1995)].

[25] I. D. Hands, J. L. Dunn, and C. A. Bates, Phys. Rev. B **63**, 245414 (2001).
[26] I. V. Rubtsov, D. V. Khudiakov, V. A. Nadtochenko, A. S. Lobach, and A. P. Moravskii, Chem. Phys. Lett. **229**, 517 (1994).
[27] I. V. Rubtsov, D. V. Khudiakov, A. P. Moravskii, and V. A. Nadtochenko, Chem. Phys. Lett. **249**, 101 (1996).
[28] R. C. Haddon, L. E. Brus, and K. Raghavachari, Chem. Phys. Lett. **125**, 459 (1986).
[29] M. C. M. O'Brien, J. Phys. C **16**, 6345 (1983).
[30] L. F. Chibotaru, J. Phys. A **27**, 6919 (1994).
[31] N. Manini and E. Tosatti, Phys. Rev. B **58**, 782 (1998).
[32] P. W. Fowler and A. Ceulemans, Mol. Phys. **54**, 767 (1985).
[33] Q. Xie, E. Pérez-Cordero, and L. Echegoyen, J. Am. Chem. Soc. **114**, 3978 (1992).